Particle Accelerators, 1988, Vol. 23, pp. 151–165
Reprints available directly from the publisher
Photocopying permitted by license only
© 1988 Gordon and Breach Science Publishers, Inc.
Printed in the United States of America

AN ANALYTICAL SIMULATION OF THE ION-ANTIPROTON INSTABILITIES IN THE CERN ANTIPROTON ACCUMULATOR

A. DAINELLI
CERN, PS Division, CH-1211, Geneva, 23, Switzerland
and
M. PUSTERLA
Dipartimento di Fisica-Sez. INFN, Universita di Padova, Via Marzolo, 8 35131 Padova, Italy

(Received March 20, 1987; in final form October 12, 1987)

A direct map method with a Mathieu approach to tune modulation is proposed and used to simulate nonlinear effects on particle motion that are generated by a beam–beam-like interaction of antiprotons with ions of the residual gas in the CERN Antiproton Accumulator. Two different Gaussian ion distributions are used, and the effects of the simulated beam–beam force on the particle motion is studied in phase space, with a particular attention to high-order nonlinear resonances.

1. INTRODUCTION

In circular accelerators or storage rings with negative beams (antiprotons or electrons), positive ions arising from ionization of residual gas molecules or positive charged microparticles can be trapped by the negative potential generated by the beam itself. In practice, the ions of the residual gas continue to accumulate until an equilibrium neutralization of about 0.998 is reached and pockets of ions are localized in a few regions of the ring where clearing out gets more difficult. When the intensity of the stacked beam becomes important, the interactions of the negative beam particles with the positive matter (ions or microparticles) can produce a systematic increase in transverse emittances. With the CERN Antiproton Accumulator (AA), a stack intensity above 10^{11} antiprotons and transverse emittances between π and 2π mm mrad (at 3.5 GeV/c) are sufficient to exhibit an abnormal growth of transverse emittances that can be related to the mechanism described above.*[1] The interaction of antiprotons with the few ion pockets (mainly protons) is very much like the beam–beam interaction in colliding-beam machines.[2]

* The average gauge pressure of the AA during normal operation is about 10^{-11} torr with 90% H_2 and 10% CO or N_2 residual gas. With this pressure each antiproton can produce with roughly the same probability an ion of H_2^+, CO^+, or N_2^+ in about 25 seconds (mean time). The neutralization process, through multiple Coulomb scattering, favors the escape of heavy ions (CO^+, N_2^+) and the final ion pocket is therefore mainly populated by protons as a result of double ionization of molecular hydrogen.

The electromagnetic field generated by the ion distribution can be described by a transcendental function that in principle contains all the powers of the transverse coordinates (x and y). The presence of all powers of these transverse coordinates in the perturbing force makes the system highly nonlinear and may explain the excitation of high-order nonlinear resonances that have been seen in the CERN AA. In this storage ring a scanning of the horizontal betatron tune (maintaining the vertical one fixed) shows the emittance growth due to the crossing of several 15th and 11th order nonlinear resonances. Some tune modulation (from ripple in the AA magnetic current) must also be added to describe this behavior. This tune-modulation amplitude is estimated to be about $A_m \simeq 3 \times 10^{-5}$, and its frequency is $\nu_s \simeq 300$ Hz. The effect described above, together with other effects due to the possible presence of SiO_2 microparticles, appear as potential limitations to the CERN AA performance; these limitations can become quite serious in the presence of higher intensities that will be reachable after completion of the CERN Antiproton Collector.[3] A good understanding of nonlinear problems in the AA seems therefore necessary.

Furthermore the AA phenomenology, as described above, could be looked at as an interesting application field for many of the general ideas of nonlinear dynamics, such as nonlinear-map instability, phase-space structure, and chaos from deterministic motion. If we describe the particle motion in a storage ring in terms of the azimuthal coordinate θ, directly proportional to the time, and we focus our attention on transverse motion, the system has only two degrees of freedom (the Hamiltonian is supposed to be independent of θ) and the phase-space behavior can be visualized without too much difficulty.

The aim of this note is to study in a detailed way the behavior of the phase space and the occurrence of nonlinear resonances for a linear system (the linear betatron motion of charged particles in storage rings) upon which a weak nonlinear perturbation (the antiproton-ion interaction) is added, with the possibility of making the antiproton dynamics in its phase space unstable.

2. DIRECT MAP FORMALISM

A rudimentary description of charged-particle transverse motion in circular machines is that of the simple harmonic oscillator; in this description every local (fine) peculiarity of the ring lattice is neglected and only the overall sinusoidal pattern is taken into account. The two coupled equations of motion (which can be derived from a classical Hamiltonian approach)[4] are

$$x''(\theta) + \nu_{ox}^2(1 - \lambda \cos \nu_\theta \theta)x(\theta) = \xi x \Phi(x, y)\Sigma_n \delta(\theta - n2\pi), \tag{1}$$

$$y''(\theta) + \nu_{oy}^2(1 - \lambda \cos \nu_\theta \theta)y(\theta) = \xi y \Phi(x, y)\Sigma_n \delta(\theta - n2\pi). \tag{1a}$$

Two types of interactions contribute to the slope variation x'' in Eq. (1). The first is the restoring force of the "rudimentary" lattice (slightly modulated). The second one represents the instantaneous kick due to the localized ion pocket, which is here assumed to occur at just a single point in the ring (and hence at every multiple of 2π in θ). We consider one interaction per turn in order to exhibit the effect qualitatively; to be more realistic one should choose a small

number of such interaction points (two, three, or four) the better to simulate the actual situation in the AA ring. The strength of the kick depends on a coupling constant, ξ, the impact parameter coordinates x, y, and the ion-pocket distribution Φ, which is nonlinear in x and y. A more detailed description of the coupling constant ξ and the Φ function in terms of electrostatic forces is given below (Section 3).

Equation (1), in the absence of the right-hand member, is the classical Mathieu equation, which, following classical textbooks, can be rewritten in terms of the new variable $z = \nu_\theta \theta/2$:

$$x''(z) + (a - 2q \cos 2z)x(z) = (2/\nu_\theta)\xi x \Phi(x, y)\Sigma_n \delta(z - n\pi\nu_\theta), \tag{2}$$

with $a = 4(\nu_x/\nu_\theta)^2 q = 2(\nu_x/\nu_\theta)^2 \lambda$. The physical system is determined completely by Eqs. (1) or (2). To obtain a numerical tool useful to follow the behavior of a particle in this system, we can derive a direct map from Eq. (2) that can give the phase-space coordinates of the particle at the $(n+1)$th turn by means of the phase-space coordinates at the nth turn.[5,6] We have then

$$x_{n+1}(n+1) = \{D_1 x_n(n) + D_2[x'_n(n) + (2/\nu_\theta)\xi x_n(n)\Phi(n)]\}/D, \tag{3}$$

$$x'_{n+1}(n+1) = \{D_3 x_n(n) + D_4[x'_n(n) + (2/\nu_\theta)\xi x_n(n)\Phi(n)]\}/D, \tag{3a}$$

and similarly for y and y', where

$$\begin{aligned} D &= M'(n)N(n) - M(n)N'(n), \\ D_1 &= M'(n)N(n+1) - M(n+1)N'(n), \\ D_2 &= M(n+1)N(n) - M(n)N(n+1), \\ D_3 &= M'(n)N'(n+1) - M'(n+1)N'(n), \\ D_4 &= M'(n+1)N(n) - M(n)N'(n+1), \end{aligned} \tag{3b}$$

with $M(n) = M(z = n\pi\nu_\theta)$ and $N(n) = N(z = n\pi\nu_\theta)$, $M(z)$ and $N(z)$ being two linearly independent solutions of the homogeneous Mathieu equation[7] (see Appendix).

3. FORCES ACTING ON ANTIPROTONS

Space-charge forces acting on antiprotons due to the beam itself can be derived from Gauss's theorem and Ampere's law;[2] with a cylindrical charge distribution we obtain

$$F_{sc}(r) = (ne^2/2\pi\varepsilon_0)(1 - \beta^2)D(r)/r. \tag{4}$$

Here n is the linear antiproton density in the beam and $\beta = v/c$; $D(r)$ depends on the chosen beam distribution and is equal to

$$D(r) = [1 - \exp(-r^2/2\sigma^2)], \tag{5}$$

with

$$\rho(r) = (ne/2\pi\sigma^2) \exp(-r^2/2\sigma^2). \tag{6}$$

With the antiproton γ value in the CERN AA ($\gamma = 3.77$), the space-charge force drops to about 7% of the electrostatic force.

When the antiprotons travel through an ion cloud somewhere in the AA ring, the radial force acting on them, due to the ion cloud, can be described by (again with cylindrical symmetry)

$$F_{\text{ions}}(r) = -\eta(ne^2/2\pi\varepsilon_0)D(r^2/2\sigma^2)/r, \tag{7}$$

in which η is the neutralization factor in the ion cloud, $n_{\text{ions}} = \eta n$ (the mean value all around the ring is of the order of 20%); the x and y components of this radial force are

$$F_x = -(x/r)\,|F_{\text{ions}}(r)| = -\eta(ne^2/2\pi\varepsilon_0)xD(r^2/2\sigma^2)/r^2, \tag{8}$$

$$F_y = -(y/r)\,|F_{\text{ions}}(r)| = -\eta(ne^2/2\pi\varepsilon_0)yD(r^2/2\sigma^2)/r^2. \tag{9}$$

For the slope deviation we can write

$$x''(\theta) = (R/\omega p)F_x, \qquad y''(\theta) = (R/\omega p)F_y, \tag{10}$$

where ω is the revolution frequency and p is the reference momentum; for the x coordinate we have

$$\begin{aligned} x''(\theta) &= -(R/\omega p)\eta(ne^2/2\pi\varepsilon_0)xD(r^2/\sigma^2)/r^2, \\ x''(\theta) &= -(nr_p/\gamma 2\sigma^2)(Rc/\omega)(1/\beta)\eta xD(r^2/\sigma^2)/(r^2/2\sigma^2). \end{aligned} \tag{11}$$

If we suppose that the change in slope is made abruptly at $\theta = k2\pi$, we can write

$$\Delta(x') = -(Nr_p/2\gamma\sigma^2)(1/\beta)R\eta x\Phi(r^2/2\sigma^2)(L/R)\Sigma_k\delta(\theta - k2\pi). \tag{12}$$

The terms $N = \int n(s)\,ds = nL$ and $\Delta\theta = L/R$ have been introduced because of dimensional considerations. We can define a coupling constant ξ and rewrite:

$$\Delta(x') = \xi x\Phi(r^2/2\sigma^2)\Sigma_k\delta(\theta - k2\pi), \tag{13}$$

$$\xi = -(Nr_p/2\gamma\sigma^2)(1/\beta)\eta L. \tag{14}$$

The change in slope $x'(\theta)$ at each $\theta = k2\pi$ is therefore:

$$\Delta(x') = \xi x\Phi(r^2/2\sigma^2). \tag{15}$$

With $\sigma \cong 1$ mm, $r_p \cong 1.5 \times 10^{-18}$ m, $N \cong 0.2 \times 10^{10}\,\bar{p}$/m, and $L = 1$ m, a realistic value of the coupling constant comes out to be of the order of 10^{-3}–10^{-2}; in this range the result is strongly dependent on the L and η values.

A more realistic distribution, still with a Gaussian shape but with $\sigma_x \neq \sigma_y$ ($\sigma_x > \sigma_y$), is

$$\rho(x, y) = (ne^2/2\pi\sigma_x\sigma_y)\exp(-x^2/2\sigma_x^2 - y^2/\sigma_y^2). \tag{16}$$

With this "elliptical" distribution the slope deviation can be written as[8]

$$\Delta(x') = \xi^* \operatorname{Im}[W(z)], \qquad \Delta(y') = \xi^* \operatorname{Re}[W(z)], \tag{17}$$

with

$$\xi^* = \xi(\pi^{1/2}/2)\sigma^2/(\sigma_x^2 - \sigma_y^2), \tag{18}$$

$$W(z) = (1/\kappa)\{w[(x + iy)\kappa] - \exp[-(x/2\sigma_x)^2 + (y/2\sigma_y)^2]w[(xr + iy/r)\kappa]\}, \tag{19}$$

$$\kappa = 1/[2(\sigma_x^2 - \sigma_y^2)]^{1/2} \qquad r = \sigma_y/\sigma_x, \tag{20}$$

where $w(z)$ is the complex error function defined as

$$w(z) = e^{-z^2}\left[1 + (2i/\pi^{1/2})\int^z e^{\zeta^2} d\zeta\right] \tag{21}$$

and can be evaluated by means of a fast computer program[9] that can be very useful in particle tracking simulations.

4. NUMERICAL SIMULATIONS

Uncoupled linear motion can be represented in phase space by the product of two independent ellipses, i.e., a torus upon which the representative point moves with time evolution.[10] The motion of the representative point upon the torus can be described by two coordinates, θ_1 and θ_2; the former coordinate is the polar coordinate on the torus cross section while the latter is just the azimuthal coordinate around the torus. If $\omega_1 = \dot{\theta}_1$ and $\omega_2 = \dot{\theta}_2$ are in a rational relationship ($m\omega_1 = n\omega_2$; m and n are integers), the representative point of the motion closes its orbit after m revolutions upon the torus; the signatures that it leaves through a plane in phase space during the first m turns are also the crossing points of the successive motion. The invariant torus is said to be rational. If ω_1 and ω_2 are not in a rational relationship, the orbit remains open forever, the trajectory of the representative point covers in a dense fashion all the torus surface, and the signature left through a plane during the motion is a continuous curve (ellipse). The invariant torus is said to be irrational.

The ratio ω_1/ω_2 (winding number) depends on the amplitude of the motion and therefore, in general, is different for distinct tori. Thus if the system is linear and unperturbed, the Hamiltonian generates, in phase-space projections, invariant curves that belong to rational or irrational winding numbers.

If a small perturbation is added, the whole picture may change and become extremely complicated; but if the perturbation is sufficiently weak, tori with irrational winding numbers do survive, although in a distorted form. On the other hand, tori with rational winding numbers are completely destroyed, and the pattern of phase-space projections are small closed curves around stable fixed points separated by diffuse regions with an unstable fixed point at each of them. These unstable fixed points are the origin of chaotic motion in phase space, i.e., motion that is extremely sensitive to initial condition.

4.1. Nonlinear Resonances

A numerical code (DIRMAP) has been derived from the direct map relationship described in Eq. (3). This simple numerical tool makes it possible to investigate some interesting aspects of charged-particle behavior in a storage ring in the presence of nonlinear forces such as those that originate from the antiproton–positive-ion interactions described above.

With two coupled degrees of freedom, nonlinear resonances in the amplitudes can be found with values of the transverse betatron tunes ν_x and ν_y that satisfy the well known resonant condition:

$$m\nu_x + n\nu_y = p, \tag{22}$$

with m, n, and p integers;[4,11,12] $q = |m| + |n|$ is called the order of the nonlinear resonance. In presence of a tune modulation with frequency ν_s, (in both planes), the resonant condition becomes

$$m\nu_x + n\nu_y = p + k\nu_s. \tag{23}$$

If the tune modulation acts on one degree of freedom (two-dimensional phase space), each resonance of order n acquires an infinite number of satellite resonances that are separated by ν_s/n and reduced in strength by the factor $J_k(n\nu/\nu_s)$, where J_k is a Bessel function of the first kind;[2,13] the resonant condition then becomes

$$\nu_x = p/n + k\nu_s/n \quad (k = 0, \pm 1, \pm 2, \ldots). \tag{24}$$

4.2. Third-Integer Resonances Driven by a Sextupolar Field

In order to test the code confidence, many numerical simulations have been done around a third-integer resonance ($\nu_x = 7/3$) driven by a sextupolar term in the force of the type $(x^2 - y^2)$ and xy. In Fig. 1 a typical result obtained with the DIRMAP code is shown. The horizontal betatron tune is incremented by fixed steps. For each horizontal betatron tune value, a sequence of 5000 map iterations is initiated. The iteration is truncated when the particle amplitude becomes greater than a fixed one (related to the physical aperture of the storage ring) and the particle itself can be considered lost. In Fig. 1 we have plotted the reciprocal of the number of iterations N as a measure of the growth rate; furthermore the strength has been normalized to be unity at the exact resonance value ($\nu_x \simeq 7/3$). The first satellite resonance described above is clearly seen at the expected value of horizontal betatron tune ($\nu_x = 2.3333 + 0.0780/3 \simeq 2.3593$).

4.3. High-Order Nonlinear Resonances Driven by Gaussian Charge Distributions

Nonlinear resonances of high order are in general very difficult to exhibit by means of simulation codes because of their weakness and consequently the low growth rate of the resonant amplitude. The overall behavior of the tune-modulated antiproton-ion potential is better understood if the betatron tune values are chosen near a relatively strong resonance such as a third-integer one. Furthermore, comparisons are possible with the case in which only quadratic terms are present in the force expression (sextupole). Also, the minimum value of the coupling constant ξ, which is necessary to make active at least the first-expansion polynomial terms of the complete Gaussian distribution, can be better determined near a third-integer resonance.

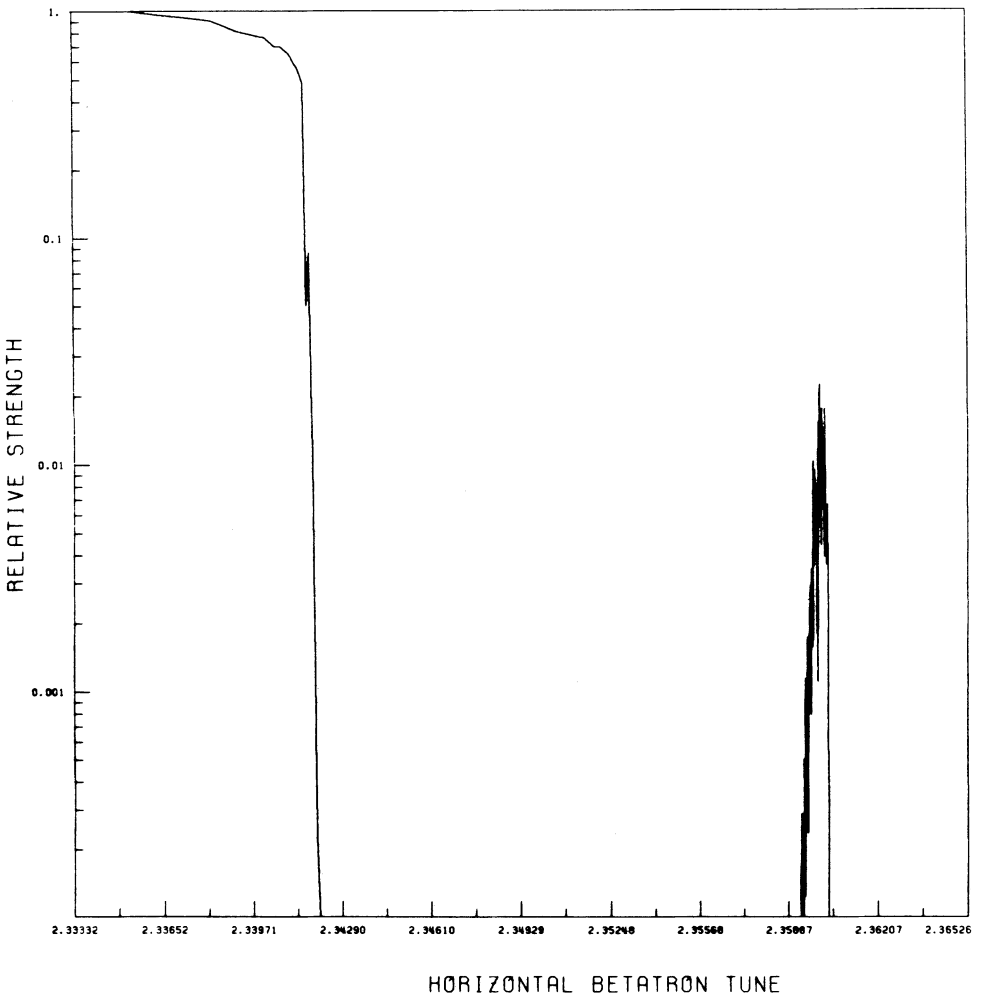

FIGURE 1 Satellite resonance near a third-integer one.

In order to realize the program described above, the even parity of the charge distribution must be destroyed at least in the x direction if we want to reproduce the odd resonances. This can be easily done by introducing a displacement x_d along the x direction. In this way all powers of x are present in the $\Phi(x, y)$ expansion, and quadratic terms $(x^2 - y^2, xy)$ appear in the kick expression as is necessary in order to excite third-integer resonances.

The first striking difference between cylindrical and elliptical charge distributions is that the latter seems more effective in producing unstable motion than the former. If one tries to use the elliptical distribution and ξ values of the order of unity with the same initial conditions in both planes already used for the cylindrical charge distribution, the motion is completely unstable and no more than 10 iterations are possible.

The second important difference is that, when an apparent stability is present (smaller ξ values), the overall behavior of motion with elliptical charge distribution is much more chaotic (diffuse) than the cylindrical one; the onset to chaotic behavior has been proved with the Liapounov exponent method.[6,14,15] Furthermore, with increasing ξ, transition from stable to unstable motion seems quite abrupt without steps with rational and irrational tori,[6] and the phase-space structure appears completely different, as shown in Fig. 2.

This completely different behavior between cylindrical and elliptical charge distribution can easily be exhibited in pictures of relative resonance strength (reciprocal of number of "turns" before the particle is lost) versus horizontal betatron tune.

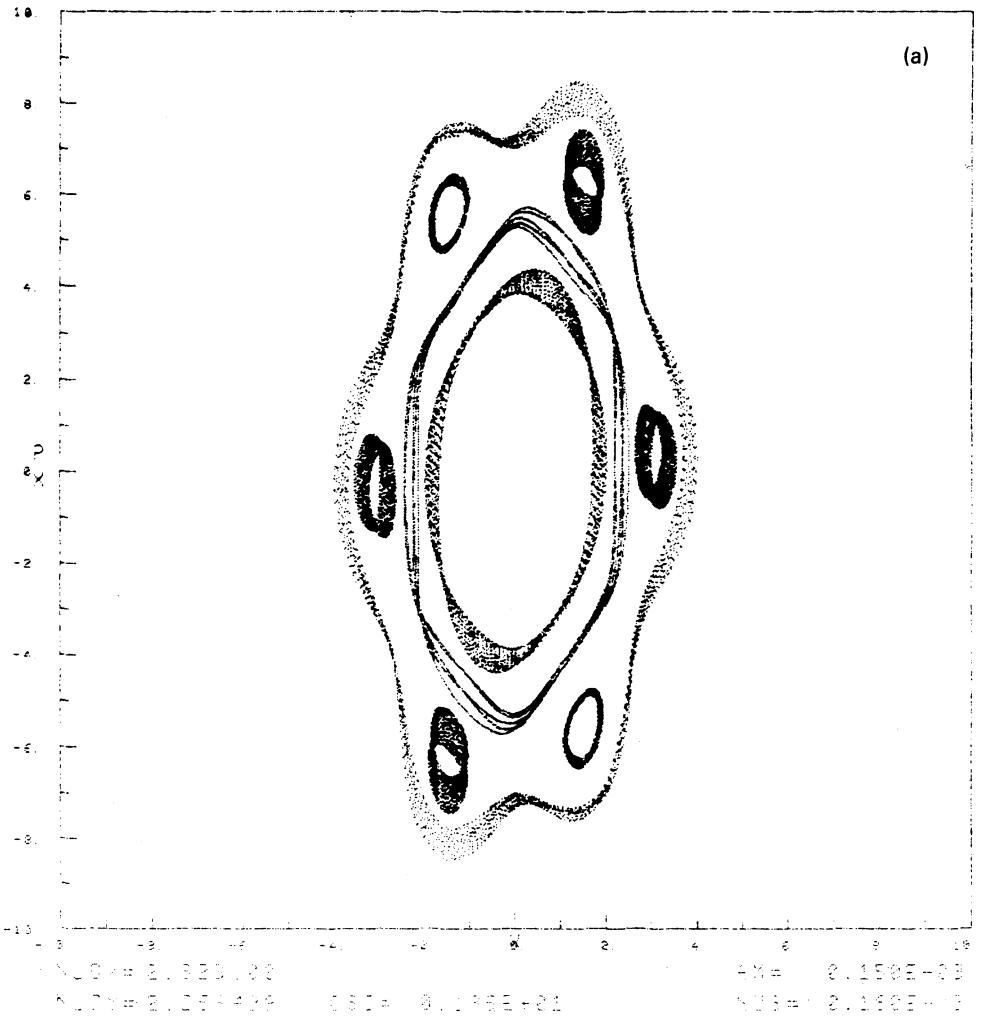

FIGURE 2 Phase-space behavior of the map with a Gaussian charge distribution; (a) cylindrical symmetry ($\sigma_x = \sigma_y$), (b) elliptical shape ($\sigma_x > \sigma_y$).

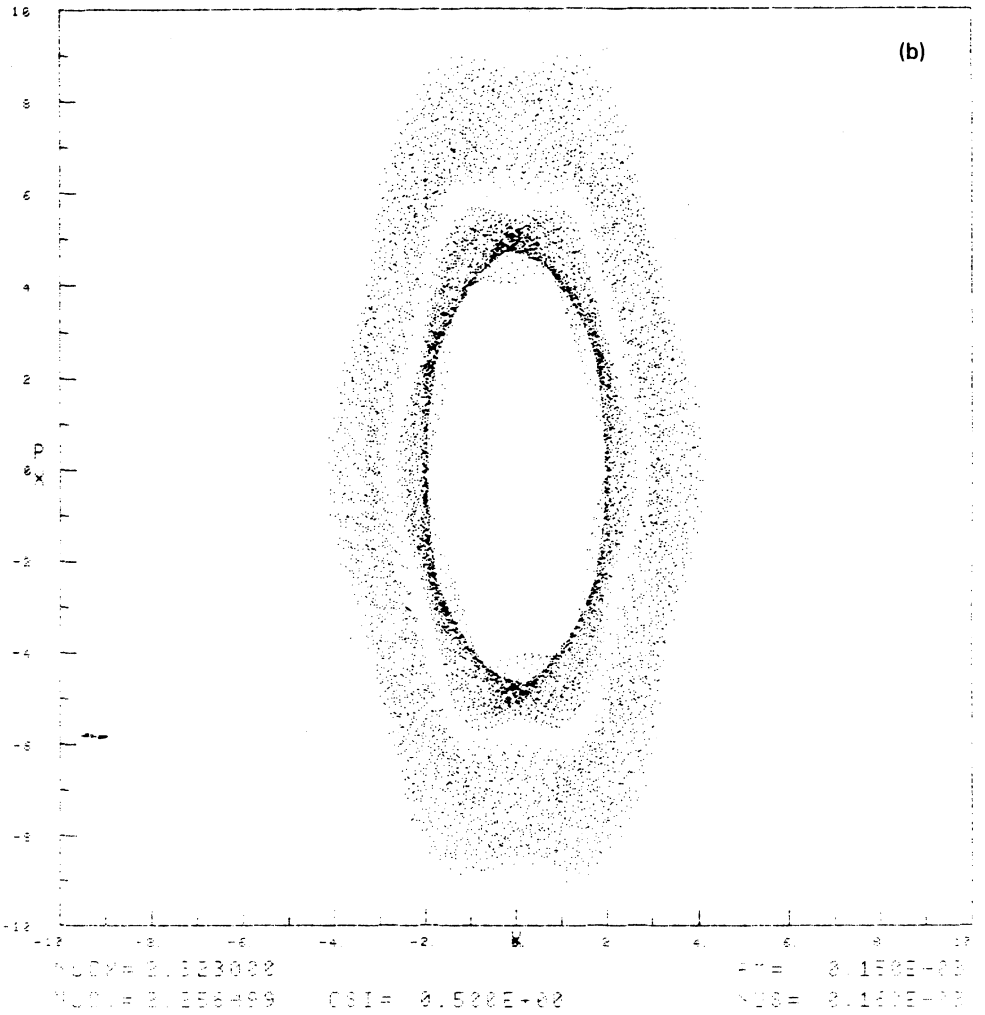

FIGURE 2 (continued)

When the cylindrical charge distribution is used, also with values of the coupling constant ξ much greater than the physical ones, the behavior of the map remains stable over most of the range where some important nonlinear resonances of even parity should appear. This stresses the relative weakness of the cylindrical charge distribution to excite nonlinear resonances. Such behavior can be seen in Fig. 3a, where the value of the coupling constant ξ is equal to $2.0\,(\simeq 100\xi_{\text{phys}})$. Because of the even parity of charge distribution, only even-order resonances can be excited. The strongest even resonance in the chosen range is the $\nu_x = 9/4$ resonance. With $\xi = 2.0$ the cylindrical distribution reproduces this peak; the same peak can be also attributed to at least two other nonlinear resonances ($2\nu_x + 2\nu_y = 9$, $\nu_x = 2.2435$; $3\nu_x + \nu_y = 9$, $\nu_x = 2.24783$). Three other peaks are reproduced by the cylindrical distribution, and their most probable identification is given in Fig. 3a.

As suggested above, the definite parity (even) of the cylindrical distribution can be destroyed by giving a displacement of quantity x_d to its center. In this way also the odd resonances can be excited; the most important one in the chosen range is $\nu_x = 7/3$. After switching on the decentralization of the charge distribution (Fig. 3b), the third-integer resonance appears and because it is stronger than the $\nu_x = 9/4$ one, it becomes the highest peak in the figure (the previous peak at 2.330 increases to 2.333); two other odd nonlinear resonances also seem to appear. Further simulations show that different odd resonances are excited with different displacements of the cylindrical charge distribution.

The corresponding pictures obtained with the elliptical charge distribution are

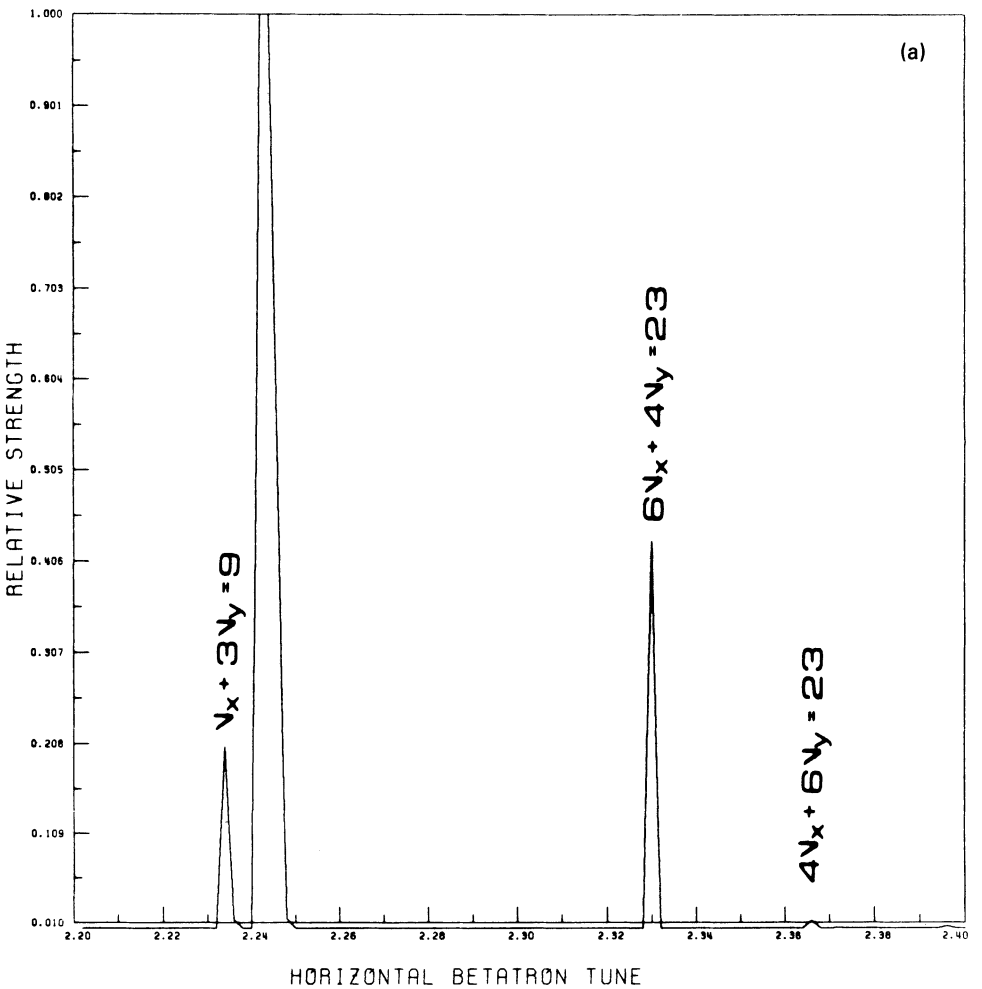

FIGURE 3 Some nonlinear resonances simulated by means of a Gaussian charge distribution ($\sigma_x = \sigma_y$ cylindrical shape) with a definite even parity in (a) and an indefinite one in (b).

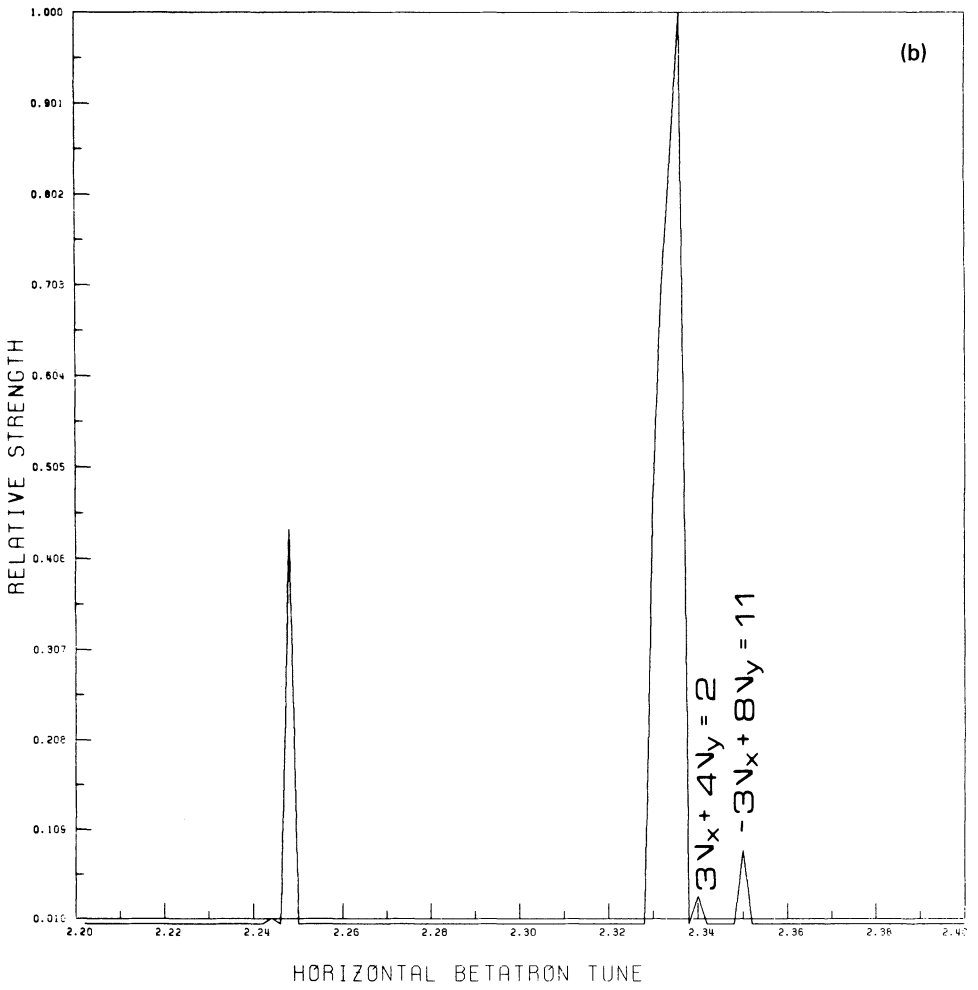

FIGURE 3 (continued)

shown in Fig. 4. Again the coupling constant ξ used here is two orders of magnitude smaller than the one used with the cylindrical distribution in Fig. 3. Two main resonances are reproduced by the elliptical distribution without decentralization. With an elliptical charge distribution, the force acting on the particle is not in the radial direction, but the same considerations on parity (even) apply because the charge distribution still has a definite even parity. Two main even resonances ($\nu_x = 9/4$, $\nu_x = 19/8$) are reproduced in Fig. 4a, in which no decentralization has been introduced. After switching on the decentralization the three main odd resonances in the range also appear ($\nu_x = 11/5$, $\nu_x = 7/3$, $\nu_x = 12/5$). Other peaks appear, and their most probable identification is given in Fig. 4b. Again, as with the cylindrical case, different odd resonances seem to be excited by different decentralizations of the charge distribution.

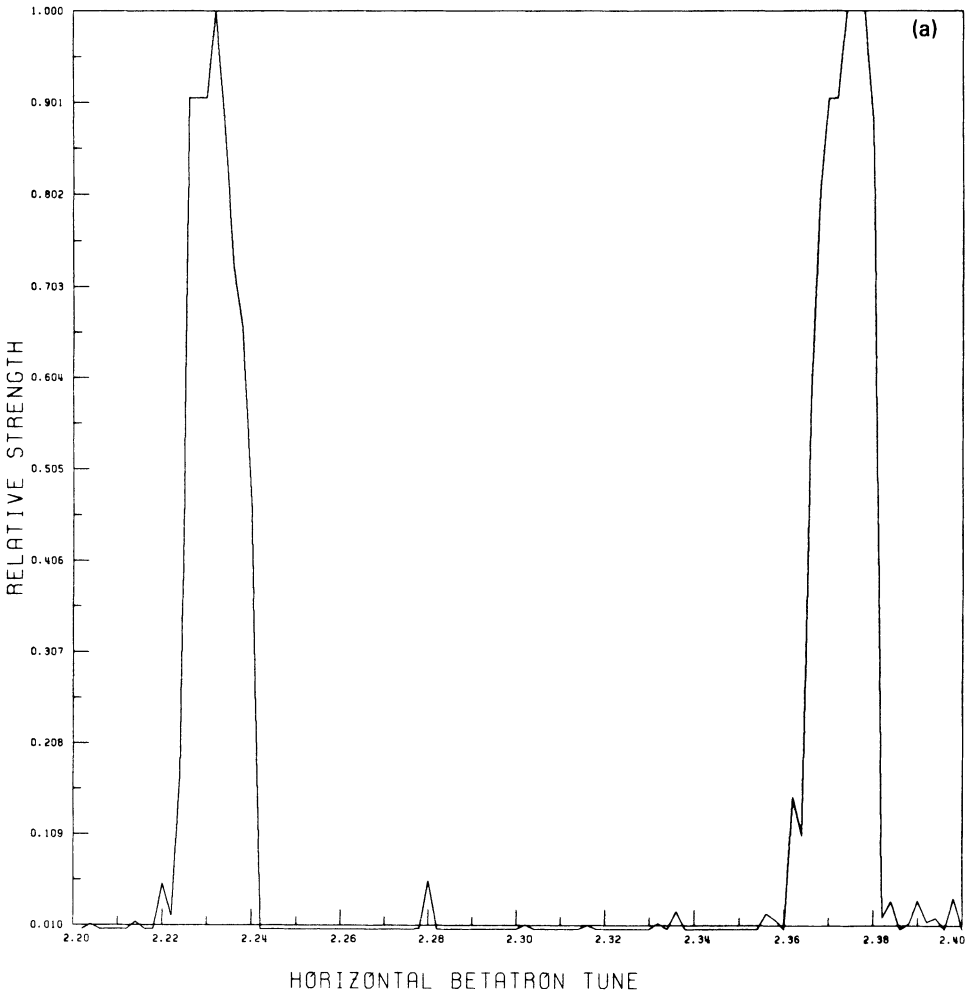

FIGURE 4 Some nonlinear resonances simulated by means of a Gaussian charge distribution ($\sigma_x > \sigma_y$, elliptical shape): (a) no decentralization introduced, (b) decentralization introduced.

5. CONCLUSION

A direct map approach seems to be a powerful way to simulate systems characterized by nonlinear dynamics such as those generated by the interaction of antiprotons with ions of residual gas (beam-beam-like interaction) in the CERN Antiproton Accumulator. The approach used here describes in a very simplified fashion the transverse betatron motion in storage rings (harmonic oscillations), and the attention is focused on the study of more interesting aspects of nonlinear coupling perturbation between x and y degrees of freedom. Furthermore, the Mathieu approach on the map appears to be adequate to include the tune modulation consistently.

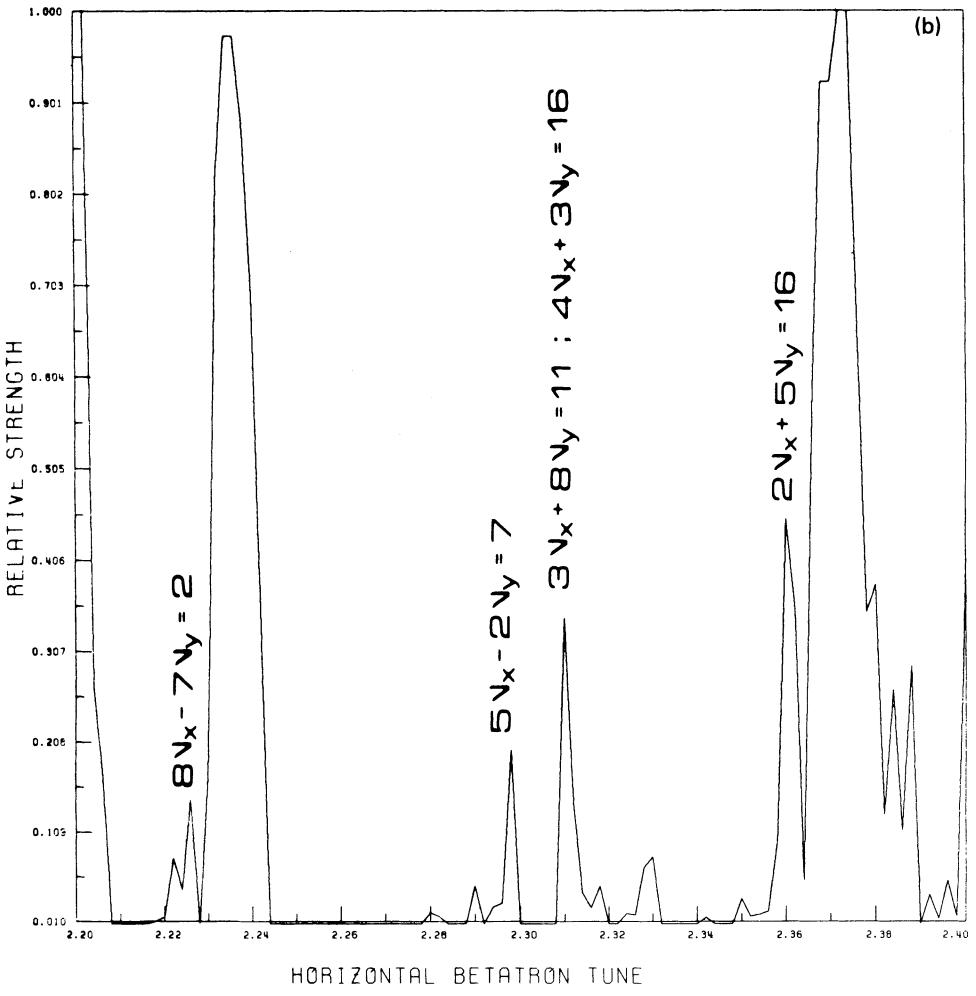

FIGURE 4 (continued)

The high number of map iterations (in short computer times) that are possible because of the extremely simplified model of transverse betatron motion is perhaps the major advantage of the direct map method used here. In this way one can directly study the phase-space structure and its evolution while some fundamental physical parameters such as betatron tunes and coupling constants of the interaction are modified. The high number of turns also allows a precise study of phase-space behavior near very weak high-order resonances and their identification.

The behavior of the map (or the motion of the particle) has been studied with different ion distributions; this study confirms that charge distributions with Gaussian shape and different standard deviations in x and y directions ("elliptical distributions"; $\sigma_x > \sigma_y$) are more effective than the cylindrical one ($\sigma_x = \sigma_y$) for the excitation of high-order nonlinear resonances. Nevertheless, not all the

expected first nonlinear resonances are reproduced by the elliptical distribution; a more refined study with the choice of an elliptical distribution of ions truncated at $x_i \simeq \sigma_i$ could be useful; this distribution can have a more physical meaning because of the incomplete neutralization of the beam. With this improvement the disagreement between the physical coupling constant and the numerical one ($\xi_{\text{phys}} \simeq 10\xi_{\text{num}}$) might be resolved.

ACKNOWLEDGMENTS

We are very grateful to Dr. E. J. N. Wilson of CERN for his continuous interest in the developments of this work and his observations, which we found very essential throughout all this research. One of us (A.D.) wishes to thank the CERN organization and in particular the Antiproton Accumulator group for their support and kind hospitality.

APPENDIX

Mathieu Functions

If $q \ll 1$, the homogeneous Mathieu equation,

$$x''(z) + (a - 2q\cos 2z)x(z) = 0, \tag{A-1}$$

has the following solutions (elliptical cosines and elliptical sines):[8]

$$\begin{aligned} M(z, q) = {} & \cos \nu z - (1/4)q[\cos(\nu+2)z/(\nu+1) - \cos(\nu-2)z/(\nu-1)] \\ & + (1/32)q^2[\cos(\nu+4)z/(\nu+1)(\nu+2) + \cos(\nu-4)z/(\nu-1)(\nu-2)] \\ & - (1/128)q^3[(\nu^2+4\nu+7)\cos(\nu+2)z/(\nu-1)(\nu+1)^3(\nu+2) \\ & - (\nu^2-4\nu+7)\cos(\nu-4)z/(\nu+1)(\nu-1)^3(\nu-2) \\ & + \cos(\nu+6)z/3(\nu+1)(\nu+2)(\nu+3) \\ & - \cos(\nu-6)z/3(\nu-1)(\nu-2)(\nu-3)] + \cdots \end{aligned} \tag{A-2}$$

$$\begin{aligned} N(z, q) = {} & \sin \nu z - (1/4)q[\sin(\nu+2)z/(\nu+1) - \sin(\nu-2)z/(\nu-1)] \\ & + (1/32)q^2[\sin(\nu+4)z/(\nu+1)(\nu+2) + \sin(\nu-4)z/(\nu-1)(\nu-2)] \\ & - (1/128)q^3[(\nu^2+4\nu+7)\sin(\nu+2)z/(\nu-1)(\nu+1)^3(\nu+2)] \\ & - (\nu^2-4\nu+7)\sin(\nu-4)z/(\nu+1)(\nu-1)^3(\nu-2) \\ & + \sin(\nu+6)z/3(\nu+1)(\nu+2)(\nu+3) \\ & - \sin(\nu-6)z/3(\nu-1)(\nu-2)(\nu-3) + \cdots \end{aligned} \tag{A-3}$$

with

$$a = \nu^2 + q^2/2(\nu^2-1) + q^4(5\nu^2+7)/32(\nu^2-1)^3(\nu^2-4)\cdots \tag{A-4}$$

If, as with the CERN AA parameters, the value of q is not less than unity ($q = 2\lambda(\nu_x/\nu_\theta)^2 \simeq 2 \times 10^4$ for AA), an approximate analytical solution can still be

obtained by means of the Liouville transform:[16]

$$\zeta = \int_0^z (a - 2q \cos 2z')^{1/2} \, dz', \tag{A-5}$$

$$x = \eta/(a - 2q \cos 2z)^{1/4}. \tag{A-6}$$

Neglecting terms of the order of $(2q/a^2)$, we obtain a new Mathieu equation in terms of the η variable with solutions that are valid when $q \gg 1$:

$$M_L(z) = (a - 2q \cos 2z^*)M(z^*), \tag{A-7}$$

$$N_L(z) = (a - 2q \cos 2z^*)N(z^*), \tag{A-8}$$

where $M(z)$ and $N(z)$ are again the elliptical cosines and elliptical sines in expressions (A-2) and (A-3) evaluated at

$$z^* \simeq z - (q/2a) \sin 2z - \cdots \tag{A-9}$$

REFERENCES

1. E. Jones *et al.*, CERN/PS/Note 85–15 (AA) (1985); *Proc. Part. Accel. Conf.*, Vancouver, B.C., 1985, *IEEE Trans. Nucl. Sci.* **NS-32** (1985).
2. L. R. Evans, *Proc. CERN Accelerator School* (Antiproton for colliding beam facilities), Geneva, CERN 84–15 (1984), p. 319.
3. E. J. N. Wilson, CERN 83–10 (1983).
4. E. D. Courant, R. D. Ruth, and W. T. Weng, SLAC-PUB 3415 (1984).
5. A. Pascolini and M. Pusterla, *Particle Accelerators* **12,** 121 (1982).
6. A. Dainelli, CERN-PS/AA/Note 86–13 (1986).
7. M. Abramowitz and I. A. Stegun, *Handbook of Functions* (National Bureau of Standards, Washington, D.C., 1966).
8. M. Bassetti and G. A. Erskine, CERN-ISR-TH/Note 80–06 (1980).
9. K. S. Kolbig, *Complex Error Function, Program C 335* (CERN, Geneva, 1970).
10. V. I. Arnold, *Mathematical Methods of Classical Mechanics* (Springer-Verlag, New York and Heidelberg, 1978).
11. E. J. N. Wilson, *Proc. CERN Accelerator School* (Advanced Accelerator Physics), Oxford, UK, September 1985 [CERN-PS/86-7(AA)].
12. A. Schoch, CERN 57–21 (1958).
13. A. Piwinsky, *IEEE Trans. Nucl. Sci.* **NS-32,** 2440 (1985).
14. H. Mais, F. Schmidt, and A. Wrulich, *Proc. Part. Accel. Conf.*, Vancouver, B.C., 1985; *IEEE Trans. Nucl. Sci.* **NS-32,** 2252 (1985).
15. R. Abraham and J. E. Marsden, *Foundations of Mechanics* (The Benjamin Co., Inc., Reading, MA (USA), 1978).
16. G. Turchetti, private communication.